QbD-driven development of intranasal lipid nanoparticles for depression treatment

Carla Vitorino[a,b,c], Soraia Silva[a,d], Filipa Gouveia[a,d], Joana Bicker[a,d], Amílcar Falcão[a,d], Ana Fortuna[a,d,*]

[a] Faculty of Pharmacy, University of Coimbra, Coimbra, Portugal
[b] Center for Neurosciences and Cell Biology (CNC), University of Coimbra, Coimbra, Portugal
[c] Coimbra Chemistry Centre, Department of Chemistry, University of Coimbra, Coimbra, Portugal
[d] CIBIT/ICNAS – Coimbra Institute for Biomedical Imaging and Translational Research, University of Coimbra, Coimbra, Portugal

ARTICLE INFO

ABSTRACT

Depression is a life-threatening psychiatric disorder and a multifactorial global public health concern. Current pharmacological treatments present limited efficacy, and are associated with several harmful side effects and development of pharmacoresistance mechanisms. Developing more effective therapeutic options is therefore a priority.

This work aims at efficiently designing an antidepressant therapeutic surrogate relying on a dual strategy supported on lipid nanoparticles and intranasal delivery. For that purpose, the formulation was comprehensively optimized following a quality by design perspective. Critical quality attributes (CQAs) ranged from physico-chemical to intranasal performance features. The optimized formulation was administered to mice in order to assess the antidepressive and anxiolytic effects by applying the forced swimming and marble-burying tests, respectively.

A cross-analysis of the predictive models established for the set of 12 CQAs elicited the formulation containing similar proportion of solid and liquid lipids and lower surfactant concentration as the optimal one. Despite increasing the liquid lipid amount yielded smaller and more homogeneous particle size, and higher release rate, nanostructured lipid carriers (NLCs) provided an earlier and superior pig nasal mucosa permeability than nanoemulsions, along with better stability and cytotoxic profiles.

Importantly, the intranasal delivery of the optimal lipid nanoparticle formulation reduced both depressive and anxiety-like behaviors, which positions these intranasal nanosystems in line with the hypothesis of provisioning timely and better acting antidepressant therapies.

1. Introduction

Depression is a life-threatening mental disorder and a major public health concern, affecting more than 300 million people of all ages worldwide [1]. It leads to disability, noteworthy health-related costs and decreased quality of life, being considered a prominent risk factor for many other diseases, including neuropsychiatric, cardiovascular, and metabolic conditions [2,3].

Conventional pharmacological treatments for depression are considered relatively well defined. Antidepressant standard-of-care comprises oral selective serotonin reuptake inhibitors (SSRIs, e.g. fluoxetine) and serotonin-norepinephrine reuptake inhibitors (SNRIs, e.g.

venlafaxine), as well as an increasing number of other types of recent antidepressants (such as bupropion and mirtazapine), besides the older tricyclic and monoamine oxidase inhibitor drugs [4–9].

Notwithstanding, the poor outcomes in terms of efficacy and safety profiles of antidepressant drugs have boosted the development of alternative delivery systems which prompt faster, better and stronger therapeutic responses, along with fewer side effects. Thus, new strategies for the treatment of depression may be directed to different routes of administration, such as the intranasal one, which has been highlighted as a reliable pathway to bypass the blood brain barrier (BBB). Indeed, the unique direct connection between the brain and the environment is mediated by the olfactory epithelium of the nasal cavity, and, hence, intranasal administration is the only non-invasive route of drug administration that may allow direct brain targeting [10]. This particular neural connection has sparked attention for delivery of a wide variety of drug molecules, ranging from small to large molecules, such as nucleotides, peptides, proteins, and even stem cells to brain. In parallel, formulation approaches have been developed to prevent enzymatic degradation and enhance the pharmacological effects, without systemic absorption and toxicity in the major peripheral organs [11]. The efficient development of drug delivery systems for intranasal administration should envision (i) increasing mucoadhesion, (ii) providing constant or controlled release of drug, (iii) improving nasal permeability, or (iv) increasing deposition at the olfactory epithelium to maximize a successful drug delivery from nose to brain [12,13].

To satisfy these assumptions, lipid nanoparticles, particularly nanostructured lipid carriers (NLCs), have been hypothesized as alternative nanosystems able to fit intranasal drug delivery purpose. NLCs are derived from o/w emulsions, wherein the liquid lipid (oil) is replaced by a mix of solid lipids (i.e., lipids that are in the solid state at both room and body temperatures) and liquid lipids, stabilized by an aqueous emulsifier(s) solution. Solid lipids can range from pure lipids to mixture of lipid compounds, comprising triglycerides, partial glycerides, fatty acids, and waxes [14]. Their biocompatibility and biodegradability, favorable physicochemical stability and controlled drug release, are characteristics that *a priori* enable them to warrant a closer contact with nasal epithelium, provisioning a faster onset and a therapeutic effect throughout longer periods of time. Additionally, the reduced costs of raw materials, ease of preparation, production not requiring organic solvents, as well as potential for manufacturing scale-up, make them attractive drug delivery systems when compared to the conventional colloidal carriers [15].

Selecting the right system to the intended purpose is not enough. The methodology "to get it right at the first time" should be a requirement. Indeed, the quality by design (QbD) approach has increasingly become the *status quo* of pharmaceutical development. This relies on a systematic, science and risk-driven methodology to design drug products that prospectively plans their desired quality features. As such, this work aims at designing a lipid nanoparticle based formulation for intranasal delivery of fluoxetine hydrochloride (FLX), as model drug, supported on a QbD strategy to efficiently find the optimal conditions to provide a drug product able to combine a faster onset of action with a sustained therapeutic effect. FLX is an inhibitor of CYP2D6 and other CYP, presenting, hence, a high potential to develop drug-drug interactions (DDI), particularly when administered by the classic oral route. Also, *in vitro* and *in vivo* studies have suggested that FLX is a substrate and an inhibitor of the efflux transporter, P-glycoprotein [16]. Indeed, knock-out animals that do not express P-glycoprotein exhibit higher brain/plasma concentration ratio than the wild-type animals. Administration of FLX by intranasal route is therefore expected to decrease the DDI at intestinal and hepatic tissues as well as to evade the BBB and the P-glycoprotein therein expressed and that has been suggested to be involved in pharmacoresistant depression. Moreover, the intranasal route also decreases drug systemic exposure, and consequently adverse effects [17]. As such, FLX is herein hypothesized as a SSRI model drug to be encapsulated within lipid nanoparticles for intranasal delivery.

2. Materials and methods

2.1. Materials

Fluoxetine hydrochloride was purchased from Jinlan Pharm-Drugs Technology Co., Limited (Hangzhou, China). Polysorbate 80 (Tween® 80) was acquired from Sigma Aldrich, Co. (St. Louis, MO, USA), while Precirol® ATO 5 (glyceryl palmitostearate, melting point: 53–56 °C), Capryol™ PGMC [Propylene glycol monocaprylate (type I) NF], Lauroglycol™ 90 and Transcutol® HP, were kindly donated by Gattefossé (Saint-Priest, Cedex, France). Cell culture media and supplements were obtained from Gibco (ThermoFisher Scientific, UK). Water was purified (Millipore) and filtered through a 0.22 μm nylon filter before use. All other reagents and solvents were from analytical or high performance liquid chromatography (HPLC) grade.

2.2. Solubility studies

First, drug-in-lipid solubility was determined as pre-formulation requirement. For the solubility study in Precirol™ ATO 5, 0.5 g of the solid lipid was previously melted at 65 °C in a controlled temperature water bath. Small amounts (ca. 2 mg) of FLX were then successively added until the saturation of the lipid was achieved [18]. For the liquid lipids, an excess of FLX was dispersed in screw-capped tubes containing the liquid compounds (1 mL each) and magnetically stirred for 48 h at 25 °C. The samples were subsequently centrifuged for 5 min at 11,740*g* in a Minispin® (Eppendorf Ibérica S.L., Madrid, Spain), and a certain volume of the clear supernatant was suitably diluted with mobile phase, filtered through a 0.22 μm membrane and analyzed by a HPLC method previously validated (Table S2). Each determination was carried out in triplicate.

2.3. Preparation of lipid nanoparticle dispersions

The lipid nanoparticles were produced by the hot high pressure homogenization technique previously optimized and described [14]. It was carried out at a temperature 10 °C higher than the melting point of the solid lipid. After melting of the lipid phase (composed by 3 g in total of different liquid and/or solid lipids, Table S1), 0.6 g of FLX was incorporated, and emulsified in 30 mL of an aqueous solution of Tween® 80 (at different concentrations, Section 2.5), at the same temperature, during 1 min with an Ultra-Turrax X1020 (Ystral GmbH, Dottingen, Germany) at 25,000 rpm.

A pre-emulsion was obtained and transferred to a pre-heated Emulsiflex® C3 (Avestin Inc, Ottawa, Canada) and processed at 1000 bar for 2.5 min. The formulation was cooled down at 4 °C during 24 h to promote matrix recrystallization and nanoparticle formation.

2.4. Characterization of FLX-nanoparticles

2.4.1. Particle size

The average particle diameter and polydispersity index (PdI) were determined by dynamic light scattering (DLS), using a Zetasizer Nano ZS (Malvern, Worcestershire, UK), at a 173° detection angle and a temperature of 25 °C. The samples were diluted 100 times with ultrapurified water, and analysed three times. The results were presented as mean ± standard deviation, as retrieved from the cumulants algorithm.

2.4.2. Zeta potential

Zeta potential (ZP) was determined by electrophoretic light scattering, also employing a Zetasizer Nano ZS (Malvern, Worcestershire, UK) apparatus at a temperature of 25 °C. Before the measurements, samples were suitably diluted (100 times) with ultrapurified water. For the ZP calculations, the Helmholtz–Smoluchowsky equation was considered.

2.4.3. Entrapment efficiency and drug loading

The drug loading (DL) and entrapment efficiency (EE) were determined by an indirect method, through the measurement of the free drug present in the aqueous phase of the dispersion [15]. Drug loading, the percentage of entrapped drug divided by total matrix lipid mass, is given by the equation (1):

$$DL(\%) = (W_{total\ drug} - W_{free\ drug})/W_{lipid} \times 100 \tag{1}$$

The entrapment efficiency, which corresponds to the amount of drug that is possible to incorporate into the lipid matrix, was determined according to the equation (2):

$$EE(\%\ ) = (W_{total\ drug} - W_{free\ drug})/W_{total\ drug} \times 100 \tag{2}$$

wherein W_{total} drug is the total amount of drug determined in the nanosystem, $W_{free\ drug}$ corresponds to the free drug amount determined in the aqueous phase, and W_{lipid} stands for the lipid phase amount.

The free drug amount was determined by ultrafiltration-centrifugation, using centrifugal filter units (Amicon® Ultra 15, Millipore, Germany) with a 50 kDa molecular weight cut-off. A certain volume of the dispersion (1 mL) was placed in the inner chamber and centrifuged at 4000 *g* for 1 h 30 at 4 °C [19]. The free drug in the aqueous phase was collected from the outer chamber of the centrifuge filter unit, appropriately diluted with mobile phase (acetonitrile:buffer pH 3.8, 38:62 v/v), filtered by a 0.22 μm membrane, and determined by the HPLC method described below.

The total drug amount was determined using a specific volume of nanoparticle dispersion adequately diluted in mobile phase and heated at 60 °C for 15 min, in order to promote the extraction of the drug from the lipid matrix. The dispersion was then centrifuged for 10 min at 11,740*g* in a Minispin® (Eppendorf Ibérica S.L., Madrid, Spain). The supernatant was collected, filtered by a 0.22 μm membrane and FLX was determined applying the same HPLC technique.

Briefly, the quantification of FLX was performed through a HPLC method using a Shimadzu LC-2010HT apparatus equipped with a quaternary pump (LC-20AD), a degasser (DGU-20A5), an auto-sampler unit (SIL-20AHT), a CTO-10AS column oven and a SPD-M20A detector. A reversed-phase LiChroCART® Purospher Star column with 3 μm particle size, 4 mm of internal diameter and 55 mm length, purchased from Merck KGaA (Darmstadt, Germany), was used to perform the chromatographic separation of FLX at 35 °C. The analysis was conducted in an isocratic mode at a flow rate of 1.0 mL/min and with a mobile phase consisting of a mixture of acetonitrile:phosphate buffer 20 mM pH 3.8 adjusted with *ortho*-phosphoric acid (38:62, v/v). The detection of FLX was carried out at 226 nm. Under these conditions, FLX was eluted at approximately 2.1 min. The obtained data was processed with a Shimadzu LC-solution version 1.12 software.

2.4.4. Rheological studies

Rheological experiments were conducted in a Haake Mars III (Thermo Scientific, Dias de Sousa, Portugal) rheometer, equipped with a Peltier system as temperature control unit. For the tests, a C35-mm cone, with an angle of 1° probe was used. Rotational measurements were carried out at 25 °C between 0.1 and 10 Pa of shear stress, in order to investigate the effect of each formulation on the Newtonian viscosity.

2.4.5. Crystallinity, structure and morphology

2.4.5.1. Differential scanning calorimetry.
Differential scanning calorimetry (DSC) analysis was performed using a DSC-204F1 Phoenix differential scanning calorimeter (Netzsch, Germany). Pure compounds and the most promising lyophilized nanoparticles (10–15 mg) were placed in aluminium crucible hermetically sealed, and empty crucible were used as reference. The samples were submitted to a heating cycle from 0 to 200 °C, at a rate of 10 °C/min, with a nitrogen purge of 20 mL/min. Through Proteus Software (Netzsch, Germany), parameters such as onset temperature (T_{on}), melting point (T_{peak}), and enthalpy (ΔH) were determined.

2.4.5.2. X-ray diffraction.
The most promising lyophilized formulations and pure compounds (solid lipid and FLX) were analyzed by X-ray diffraction using a MiniFlex 600 X-ray diffractometer (Rigaku, Tokio – Japan), with CuKα radiation at 40 kV and 15 mA. The 2θ scan range was 3–50° with a step size of 0.01° and a scan speed of 5 s.

2.4.5.3. Attenuated total reflectance Fourier transform infrared.
Attenuated total reflectance Fourier transform infrared (ATR-FTIR) spectra of the most promising lyophilized formulations were recorded using a FT-IR/FT-NIR spectrometer (Spectrum 400, Perkin-Elmer, MA, USA) with an ATR accessory fitted with a Zn-Se crystal plate. The pure compounds (solid lipid and FLX) and lyophilized formulations were placed in the ATR device and measured using 32 scans for each spectrum, with a resolution of 2 cm^{-1} and a scan speed of 1 cm/s. The spectra were collected between 4000 and 650 cm^{-1}.

2.4.5.4. Transmission electron microscopy.
The morphological analyses of the most promising formulations were conducted by TEM, using the procedure reported in [20]. Briefly, the mesh grid was immersed in alcian blue at 1% (w/V) during 10 min, suitably washed, and further stained in contact with the mesh grid for 1 min. A drop of the pretreated sample was then placed in a mesh grid and dried before visualization. Observations were carried out on a Tecnai G2 Spirit BioTWIN transmission electron microscope at 100 kV.

2.4.6. In vitro release studies

In vitro release studies were performed using the static vertical Franz diffusion cells (PermeGear, Inc., PA, USA) with a diffusion area of 0.636 cm^2 and a receptor compartment of 5 mL. A dialysis cellulose membrane (MWCO ~ 12,000, average flat width 33 mm, D9652, Sigma-Aldrich), as artificial membrane, was placed between both compartments, and a receptor solution composed of phosphate buffer at a pH of 6 was used, ensuring sink conditions. This receptor compartment was stirred at 600 rpm and maintained at 34 ± 0.5 °C by a thermostatic water pump, which circulated water through each chamber jacket, mimicking nasal mucosa conditions. Formulations were applied in the donor compartment (200 μL, ca. 20 mg/mL). Subsequently, 300 μL of receptor medium was collected at 5, 15, 30, 60, 90, 120, 240, 360, 480 and 1440 min, and immediately replaced with the same volume of fresh solution. Withdrawn samples were analyzed for the drug content using the HPLC method described in **Section 2.4.3**.

2.4.7. Ex vivo permeation studies: nasal mucosa preparation and integrity test

Ex vivo permeation studies were performed in static vertical Franz diffusion cells, under the same conditions of the *in vitro* release studies, but using pig nasal mucosa instead of the dialysis cellulose membrane. The fresh membrane was provided by a local slaughterhouse (Incarpo, Condeixa, Portugal). Briefly, on the experimental day, nasal tissue was carefully harvested from olfactory bulb region of pig, and immersed in phosphate buffer pH 6. Afterward, it was cut to appropriate size and clamped between the donor and receptor compartments, with the olfactory bulb region side facing up. Again, 200 μL (ca. 20 mg/mL) of formulations were placed in the donor compartment, and 300 μL of receptor medium were removed at designated time points (5, 15, 30, 60, 90, 120, 240, 360, 480 and 1440 min). The receptor medium was immediately replenished with the same volume of fresh solution. FLX present in samples was quantified by HPLC. Permeation profiles were obtained by plotting the cumulative amount of permeated FLX against time.

According to Fick's first law of diffusion, the steady state flux (μg/cm2/h), Jss, was obtained from equation (3):

$$Jss = DC\ P/h = C\ Kp \tag{3}$$

wherein D is the diffusion coefficient of the drug in the nasal mucosa, C represents the drug concentration in the donor compartment, P is the

Table 1
Experimental design independent variables and respective codification.

Critical formulation attributes	Independent variables	Level −1	Level 0	Level +1
Liquid:solid lipid ratio	X_1	50:50	75:25	100:0
Surfactant concentration (%w/w)	X_2	2.5	3.75	5

partition coefficient between vehicle and the nasal mucosa, h is the diffusional path length, and Kp stands for the permeability coefficient. The permeability coefficient, Kp (cm/h), of FLX from each formulation was calculated by dividing the slope of the straight line portion of the curve (flux, Jss) by drug concentration originally added in the lipid nanoparticle formulations. The lag time was determined from the X-intercept of the linear portion of the graph.

2.5. Experimental design

A three-level full factorial design, 3^k, with two-variables was used for the optimization of the lipid nanoparticle based formulation. The k factors were considered, each at 3 levels, including a low, an intermediate and a high level, coded as −1, 0 and +1 level, respectively (Table 1). The inclusion of the central point is proposed to understand the model curvature in the response function, also enabling the inspection of a quadratic relationship between the responses and each of the factors [21]. The choice of variables is of utmost importance, as it conditions the experimental results and respective interpretation. As independent variables, two critical formulation attributes were considered, namely, liquid:solid lipid ratio and surfactant concentration.

As dependent variables or responses, particle size, polydispersity index, zeta potential, entrapment efficiency, drug loading, percentage of FLX released at 8 h and 24 h, amount of FLX permeated at 8 h and 24 h, permeation flow rate, permeability coefficient, and t_{lag} were analyzed. Viscosity and stability parameters (instability index and velocity of separation) were complementary assessed. Both Student *t*-test and ANOVA were performed to inspect if the terms were statistically significant in the regression model and to assess the validity of the models fitting, respectively. In the former, a 95% level of confidence (α = 0.05) was established, while in ANOVA, a value of $p < 0.05$ was considered statistically significant. Additionally, the optimal conditions were selected on the basis of the quadratic polynomial function 4

$$Y = \beta0 + \beta1x1 + \beta2x2 + \beta12x1x2 + \beta11x11^2 + \beta22x22^2 \qquad (4)$$

wherein, Y is the measured response associated with each factor level combination, β0 is the response in the absence of effects, β1 and β2 are the linear coefficients of the respective factors, β12 is the interaction coefficient between the two factors, and β11 and β22 are quadratic coefficients from the observed experimental values of Y from experimental runs that allow the prediction of the curvature of the model.

The fitted models were retrieved using JMP Pro 14 Software (Cary, NC).

2.6. Stability studies

The stability of formulations was evaluated through analytical centrifugation, using the LUMiFuge (L.U.M. GmbH, Germany) stability analyzer, which measures the intensity of transmitted near infrared (NIR) light during the centrifugation of the sample [22]. The analytical centrifugation provides an early assessment of possible instability phenomena. By measuring separation processes, e.g. flocculation, coalescence, creaming, sedimentation, it enables a rapid and accurate means of assessing dispersion stability. Such information was extracted from the analysis of transmission profiles, using the SEPView software v 6 (LUM GmbH, Berlin, Germany), from which the instability index and the velocity of separation were calculated. Briefly, instability index determines the clarification in transmission taking into consideration the particle size and the separation process at a given time in the presence of accelerated gravitational force, divided by the maximum clarification evidenced. The clarification is ascribed to the increase in transmission or decrease in particle concentration stemming from the movement of nanoparticles towards the bottom of the cell or to the cream layer [23]. The instability index is a dimensionless number between 0 and 1, wherein measurements closer to "0" stand to higher sample stability. In turn, velocity of separation (μm/s) is estimated from the linear regression of the clarification zone and according to the main instability phenomena detected (creaming or sedimentation) throughout the time of centrifugation. A higher velocity of separation reflects a higher sample instability [24–26]. The analysis of the formulations was carried out for 3 h 30 min of centrifugation, at an acceleration of 2300g and a temperature of 25 °C.

2.7. Cell viability studies

The human tumor cell line from nasal squamous epithelium (septum, RPMI 2650, ECACC 88031602) was used to assess the influence of the formulation on cell viability resorting to the Alamar Blue assay [27]. The cells were cultured in Minimum Essential Medium Eagle (EMEM, M2279) supplemented with 2 mM glutamine, 1% non-essential amino acids, 1% penicillin–streptomycin mixture and 10% heat-inactivated fetal bovine serum (Gibco Life Technologies, ThermoFisher Scientific, Waltham, MA, USA). Cells were grown in T75 flasks (Orange Scientific, Braine-l'Alleud, Belgium), passaged twice a week using a 0.25% trypsin-EDTA solution and cultured at 37 °C in 5% CO_2 and 95% relative humidity. All assays were performed with RPMI 2650 cells with passage numbers below 30.

RPMI 2650 cells were seeded into 96-well plates (Orange Scientific Braine-l'Alleud, Belgium) at a density of 6.0×10^4 cells/well and cultured for 24 h in a humidified incubator at 37 °C in 5% CO_2. After removing the culture medium, cells were incubated for 24 h with 200 μL of fresh medium (control cells), with vehicle (water) or with unloaded and FLX loaded lipid nanoparticle formulations previously selected based on their technological characteristics, permeability and stability performance (F1, F4 and F7 unloaded or loaded with FLX, see Section 3.2). A dilution series with cell culture medium, ranging from 1/4 to 1/16 000, were tested. Thereafter, treatment solutions were removed and fresh medium with 10% Alamar Blue solution (125 mg/mL) was added, followed by an incubation for 3 h. Fluorescence was measured (excitation and emission wavelengths of 530/590 nm) on a Biotek Synergy HT microplate reader (Biotek Instruments®, Winooski, VT, USA). Cell viability was calculated according to equation (5)

$$Cell\ viability(\%) = \frac{Fl - Fl_{blank}}{Fl_{control} - Fl_{blank}} \times 100 \qquad (5)$$

where Fl is the mean fluorescence observed after incubation with vehicle or each nanoformulation, $Fl_{control}$ is the mean fluorescence observed in control wells and Fl_{blank} is the mean fluorescence observed in wells containing cell medium with no cells. From these results, the 50% inhibitory concentration (IC_{50}) was defined for the nanoformulations. Vehicle concentrations were not considered to compromise cell viability if it was maintained above 70% compared with control cells [28].

2.8. In vivo studies

2.8.1. Animals and ethical considerations

Healthy adult CD1 mice weighing 30–35 g were acquired from Charles River Laboratories (L'Arbresle, France). The animals were housed in a controlled environment (12-hour light/dark cycle; temperature 20 ± 2 °C; relative humidity 55 ± 5%) for at least 7 days prior to the beginning of the experiments, with *ad libitum* access to food (4RF21, Mucedola®, Italy) and tap water. Mice were housed in a
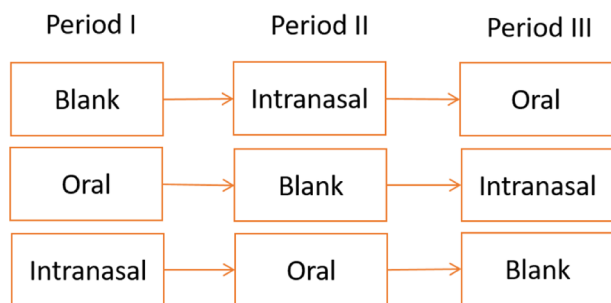
Fig. 1. Latin square design considered for the behavioral studies.

reversed light–dark cycle and were always tested in the dark phase (active phase between 08 h 00 and 20 h 00).

All experimental and care procedures were conducted in accordance with the European Directive (2010/63/EU) regarding the protection of laboratory animals used for scientific purposes and with the Portuguese law on animal welfare (Decreto-Lei 113/2013). The experimental procedures were reviewed and approved by the Portuguese National Authority for Animal Health, Phytosanitation and Food Safety (DGAV – Direção-Geral de Alimentação e Veterinária, Lisbon, Portugal, project reference 0421/000/000/2016). All efforts were made to minimize the number of animals used and their suffering.

2.8.2. Behavioral tests

In order to study the anxiety-like and depressive behavior induced by the most promising nanoformulation selected based on the aforementioned screening program, considering colloidal, loading, and performance parameters, mice marble-burying test (MBT) and mice forced swimming (FST) were performed, respectively. A Latin square design was considered for the studies to reduce response intra-variability. This consisted in three groups (*n* = 7) and three periods interspersed by three-day washing-out times (Fig. 1). All animals were pre-anesthetized by isoflurane (BBraun, Portugal) inhalation in the three periods. Mice in blank group corresponded to no treatment, mice in the oral group were administered with a FLX solution (20 mg/kg of a 2 mg/mL FLX aqueous solution containing 0.1% of Tween® 80) by gavage, while mice in intranasal group received 15 μL of nanoformulation (containing 20 mg/mL FLX, yielding an administration dose of 1 mg/kg) delivered through a catheter. One hour after drug administration, mice were sequentially and individually tested in the MBT and FST.

2.8.2.1. Marble-burying test. Selective inhibition of marble burying in mice has often been used as test for anxiolytic behavior due to the anxiogenic stimuli provided by the light reflexed through the marbles [29–31]. Additionally, marble-burying behavior of mice has been associated to potential obsessive–compulsive behaviour antagonist effects, being often used to screen anti-compulsive drugs with a high predictive ability and good face validity [32]. Attempting to assess the anxiolytic and potential obsessive–compulsive effects prompted by the antidepressant drug (FLX), marble-burying test was performed in mice administered with oral FLX solution and intranasal lipid nanoparticles encapsulating FLX, and compared with mice without treatment (Fig. 1).

The day before the test, mice were habituated to the experimental transparent polycarbonate cage (23 × 17 × 14 cm) in the absence of the marbles and all the experiments were carried out during the dark cycle. The experiment was initiated by allocating each mouse in the experimental cage containing 25 clear glass marbles of 1.5-cm diameter evenly spaced in three lines on top of 2.5-cm-deep corn cob grade 12 (Ultragene®, Santa Comba Dão, Portugal) and allowing them 30 min to explore. After returning the animals to their home cages, the unburied marbles were counted by two separate observers. According to scientific literature [31,33], marbles are considered to be buried when at least two thirds of their size was covered with sawdust. The inhibition

percentage was calculated according to the Eq. (6) [33]:

Inhibition (%) =

(number of buried marbles in control group - number of buried marbles in drug-treated group)/number of buried marbles in control group × 100   (6)

2.8.2.2. Forced swimming test. Also known as the Porsolt's test, the FST has been the most widely used paradigm to assess depression and antidepression-like behavior [34–36]. Accordingly, mice were gently placed in a transparent Plexiglas cylinder (30 cm height × 20 cm width) filled with water (15 cm from the bottom), set at room temperature (23–25 °C). Although motion was recorded for 6 min, only the last 4 min were considered for analysis, because most mice are very active at the beginning of the FST, and the potential effects of the treatment can be obscured during the first two minutes [37]. During the behavioral analysis, the time that each mouse spends mobile is measured and the immobility time is estimated by subtracting the total amount of mobility time from the 240 s of test time. Mobility was herein considered as any movements other than those required to balance the body and keep the head above the water. Furthermore, swimming time and climbing time were also registered: the first was considered if movement of forelimbs or hind limbs in a paddling fashion was observed, while the second was attributed to quick movements of the forelimbs observed such that the front paws broke the surface of the water [37,38]. Videos were observed twice and by two analysers.

The percent inhibition was calculated according to the equation (7):

Inhibition (%)

= (immobility time of control group − immobility time of drug-treated group) /immobility time of control group × 100   (7)

At the end of each test, the animals were gently removed from the water by the tail, dried with a warmed towel and placed back into their cage. The water was replaced after every session to avoid any influence on the next mouse.

3. Results and discussion

An optimization process supported on a QbD approach was applied to the development of intranasal lipid nanoparticle formulation. For that, a quality target product profile was first established (Table 2).

In addition, considering that the development of intranasal lipid nanoparticle formulations is inherently associated to several critical stages that can compromise the quality of the final product, an overall risk analysis of the factors that can potentially impact the quality of FLX lipid nanoparticles was traced by the Ishikawa diagram presented in Fig. 2. With particular emphasis on lipid nanoparticles composition, the risk ascribed to the influence of several critical material attributes (CMAs) on critical quality attributes (CQAs) was subsequently ranked according to a risk matrix, based on prior knowledge (Fig. 3). Critical process parameters were not herein included, since lipid nanoparticles were produced based on the hot high pressure homogenization technique that was previously optimized by our group, as described by

Table 2
Quality target product profile.

QTPP	Target
Dosage form	Nanosuspension based on lipid nanoparticles
Route of administration	Intranasal
Indication	Depression, pharmacorresistent depression (Model drug: fluoxetine hydrochloride, SSRI)
Stability	Long-term physicochemical stability
Impurities	As per ICH guidelines
Release	Targeted to brain
Materials	Non-toxic, biocompatible and biodegradable
Particle size	Ideally 50–150 nm
Zeta potential	Higher than |30| mV
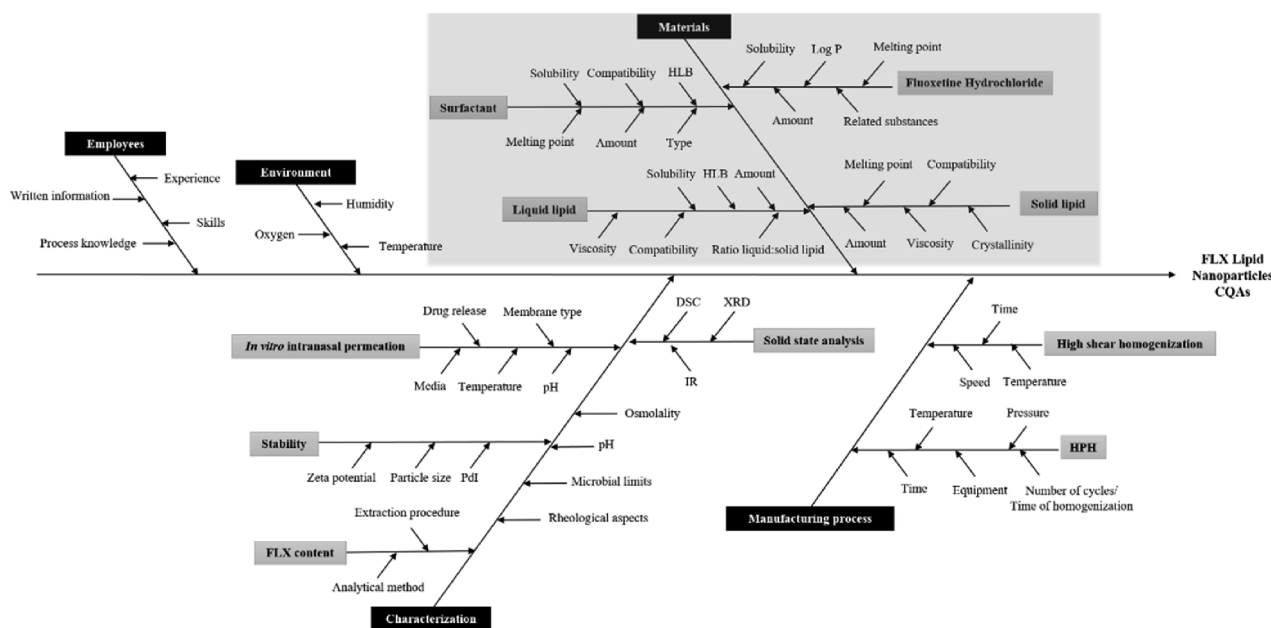
Fig. 2. Ishikawa diagram indicating critical parameters affecting lipid nanoparticle development. Key: FLX, Fluoxetine hydrochloride, DSC, Differential scanning calorimetry; EE, Encapsulation efficiency; HLB, Hydrophilic-lipophilic balance; HPH, High pressure homogenization; IR, Infrared spectroscopy; Log P, Octanol-water partition coefficient; PdI, Polydispersity index; XRD, X-ray diffraction. .
Adapted from [39]

		Drug Product CQAs								Criticality
		Particle size	**PdI**	**ZP**	**EE**	**DL**	**Stability**	**Drug release**	**Permation flux**	
CMAs	**Drug solubility**	Low	Low	Medium	High	High	Medium	High	High	++
	Drug concentration	Medium	Medium	Medium	High	High	Medium	Medium	Medium	+
	Lipids composition	Medium	Low	Low	High	High	High	High	High	++
	Lipids concentration	Medium	Medium	Medium	High	High	Medium	Medium	Medium	+
	Liquid:solid lipid ratio	High	High	High	High	High	High	High	High	+++
	Surfactant type	Medium	Medium	High	Medium	Medium	High	Low	Medium	+
	Surfactant HLB	High	High	High	High	High	High	Low	Medium	+++
	Surfactant concentration	High	High	High	High	High	High	Medium	Medium	+++

Fig. 3. Risk estimation matrix exhibiting initial risk assessment levels of individual formulation and manufacturing parameters: Low: low risk parameter; Medium: medium risk parameter, High: high risk parameter. Key: CQAs, Critical quality attributes; CMAs, Critical material attributes; PdI, Polydispersity index; ZP, zeta potential; EE, Encapsulation efficiency; DL, drug loading; HLB, Hydrophilic-lipophilic balance. .
Adapted from [39]

Table 3
FLX solubility in the tested liquid lipids (n = 3).

Liquid lipid/compound	Solubility (mg/mL)
Capryol™ PGMC	17 ± 3
Lauroglycol™ 90	21 ± 2
Transcutol® HP	206 ± 141

Mendes et al [15].

To develop the intranasal nanoparticles loading FLX applying the aforementioned rational, pre-screening solubility studies had to be performed for the selection of the appropriate lipid matrix, as it will be detailed in Section 3.1. After choosing the lipid matrix, experimental design was conducted to produce nanoparticle formulations which were

then screened regarding colloidal characteristics, permeability, stability and impact on the viability of RPMI 2650 cells. These results are discussed in the following sections, explaining the selection of the formulation F1 to be administered to mice.

3.1. Pre-screening solubility studies

Developing a formulation demands *a priori* the selection of pharmaceutically acceptable, non-irritating, and non-sensitizing excipients. They should be generally regarded as safe (GRAS status) and appropriate for the delivery route [40]. The screening of the components for the preparation of lipid nanoparticles is not an exception, requiring the stepwise selection of solid and liquid lipid or oil, based on the relative FLX solubility. Solubility of drug in the lipids is considered a precondition of encapsulation efficiency and it is expected that a high lipid

Table 4
Composition of lipid (NLC and NE) nanoparticle formulations and respective physicochemical characterization, and evaluation of their performance.

F	Lipid phase		Aqueous phase		FLX	PS	PI	ZP	EE	DL
	Precirol® % (w/w)	Lauroglycol™ 90 % (w/w)	Tween® 80 % (w/w)	Water	% (w/w)	nm		mV	%	%
1	5	5	2.5	85.5	2	154 ± 2	0.514	19.7 ± 0.5	74 ± 2	12.9 ± 0.5
2	5	5	3.75	84.25	2	142.5 ± 0.2	0.496	18.3 ± 0.4	70 ± 6	11.0 ± 0.8
3	5	5	5	83	2	132 ± 2	0.464	18.6 ± 0.7	77.7 ± 0.5	14.1 ± 0.4
4	2.5	7.5	2.5	85.5	2	158 ± 2	0.332	20 ± 1	77 ± 7	13 ± 3
5	2.5	7.5	3.75	84.25	2	115.7 ± 0.9	0.444	20 ± 1	79 ± 3	14 ± 1
6	2.5	7.5	5	83	2	91.5 ± 0.4	0.396	24 ± 1	82 ± 2	14 ± 1
7	0	10	2.5	85.5	2	128 ± 1	0.117	37 ± 1	80.1 ± 0.1	14.71 ± 0.03
8	0	10	3.75	84.25	2	119 ± 2	0.165	36.1 ± 0.8	82 ± 2	15 ± 1
9	0	10	5	83	2	100 ± 2	0.179	26.9 ± 0.1	83 ± 1	14 ± 1

F	R8h	R24h	Q8h	Q24h	Jss	Kp	t_{lag}	Viscosity
	%	%	µg.cm^{-2}	µg.cm^{-2}	µg.cm^{-2}.h	cm.h^{-1}	h	mPa.s, T = 34°C
1	27.2 ± 1.5	39.4 ± 1.6	106 ± 8	6.0 ± 0.4	807 ± 71	1314 ± 64	0.4 ± 0.2	5.589
2	27 ± 2	43 ± 4	79 ± 11	5.0 ± 0.7	600 ± 97	1073 ± 138	0.5 ± 0.2	4.619
3	22.7 ± 1.5	31 ± 2	75 ± 10	4.1 ± 0.5	106 ± 28	1035 ± 52	1 ± 1	6.154
4	26 ± 5	32 ± 12	92 ± 11	4.8 ± 0.6	644 ± 92	941 ± 102	0.4 ± 0.1	3.669
5	26.2 ± 1.6	36 ± 2	68 ± 9	3.8 ± 0.5	416 ± 76	739 ± 101	0.6 ± 0.1	4.366
6	23.4 ± 1.5	31 ± 6	45 ± 5	2.6 ± 0.3	398 ± 54	691 ± 70	1.01 ± 0.07	5.995
7	33 ± 2	42 ± 2	79 ± 10	4.3 ± 0.6	611 ± 93	1035 ± 143	0.7 ± 0.2	2.685
8	28 ± 3	35 ± 4	80 ± 14	4.2 ± 0.7	526 ± 87	1005 ± 171	0.6 ± 0.3	3.759
9	29 ± 2	37 ± 6	71 ± 12	4.5 ± 0.8	504 ± 94	836 ± 88	0.8 ± 0.1	7.632

Table 5
Coefficient values for particle size (PS), polydispersity index (PdI), zeta potential (ZP), entrapment efficiency (EE), drug loading (DL), percentage of FLX released at 8 h (%R8h) and 24 h (%R24h), cumulative amount of FLX permeated at 8 h (Q8h) and 24 h (Q24h), permeation rate (Jss), permeability coefficient (Kp), and latency time (t_{lag}), and respective summary of fit of the selected critical material attributes.* Statistical significant coefficients, as extracted from Student's *t*-test analysis.

	PS	Prob > |t|	PdI	Prob > |t|	ZP	Prob > |t|	EE	Prob > |t|	DL	Prob > |t|
β0	120.7900	< 0.0001*	0.4137	< 0.0001*	21.5741	< 0.0001*	77.9350	< 0.0001*	13.5732	< 0.0001*
β1	−13.5810	< 0.0001*	−0.1688	< 0.0001*	7.27780	< 0.0001*	3.8526	0.0023*	0.9071	0.0428*
β2	−19.2460	< 0.0001*	0.0127	0.0889	−1.1778	0.0794	1.8155	0.0954	0.2113	0.6073
β12	−1.6220	0.5709	0.0283	0.0040*	−2.3000	0.0078*	−0.3128	0.8033	−0.4934	0.3342
β11	7.5490	0.0719	−0.0678	< 0.0001*	4.8556	0.0003*	−1.5108	0.4015	−0.3718	0.6017
β22	1.3210	0.7435	−0.0348	0.0102*	−0.4444	0.6920	1.8597	0.3055	0.5863	0.4144
Multiple R^2	0.8384		0.9668		0.8848		0.6849		0.4425	

	%R8h	Prob > |t|	Q8h	Prob > |t|	Jss	Prob > |t|	Kp	Prob > |t|	t_{lag}	Prob > |t|
β0	24.981	< 0.0001*	430.3262	< 0.0001*	66.4737	< 0.0001*	3.6820	< 0.0001*	0.7964	0.0038*
β1	1.8978	0.0442*	−64.1074	0.0589	−5.0772	0.2351	−0.3526	0.1448	0.3216	0.0325*
β2	−2.2933	0.0175*	−91.4218	0.0074*	−14.6778	0.0010*	−0.6710	0.0063*	−0.0555	0.7012
β12	0.5700	0.6382	21.9215	0.5885	5.8742	0.2581	0.5298	0.0732	0.2848	0.1149
β11	3.0033	0.0288*	122.8507	0.0338*	13.3927	0.0677	0.9521	0.0225*	−0.2871	0.2518
β22	0.3867	0.7632	83.7532	0.1486	2.2978	0.7534	0.0595	0.8851	−0.1838	0.4680
Multiple R^2	0.6028		0.2966		0.2953		0.3021		0.1616	
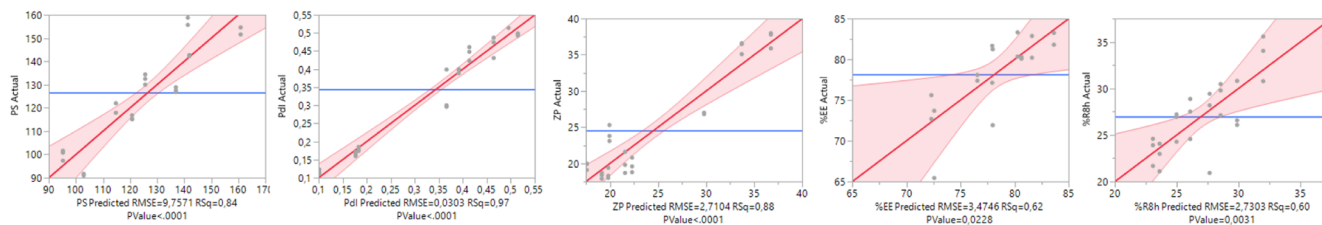
Fig. 4. Actual by predicted plots for the responses (CQAs) presenting a better goodness of fit. The diagonal line corresponds to the Y = X line. For a perfect fit, all the points would be on this diagonal. The horizontal line indicates the mean of each response (Y-residuals). Confidence curves for the line of fit are shown on leverage plots. These curves provide a visual indication of whether the test of interest is significant at the 5% level. If the confidence region between the curves contains the horizontal line representing the hypothesis, the effect is not considered significant. If the curves cross the line, the effect is significant, as observed for the majority of the responses.

solubility will determine a high encapsulation efficiency.

The choice of Precirol™ ATO 5 as solid lipid relied on the fact of being a glyceride with an intermediate melting point (~56 °C), consequently demanding lower thermal stress, and providing a reasonable FLX solubilising potential (45 ± 5 mg/g). Moreover, it is already reported biocompatibility and acceptability for nose-to-brain delivery of Precirol™ ATO 5, which favours its selection for the present study [41]. To further maximize loading properties, different liquid lipids with distinct hydrophilic-lipophilic balance (HLB) values (Table 3) were selected and the respective FLX solubility was assessed (Table 3).
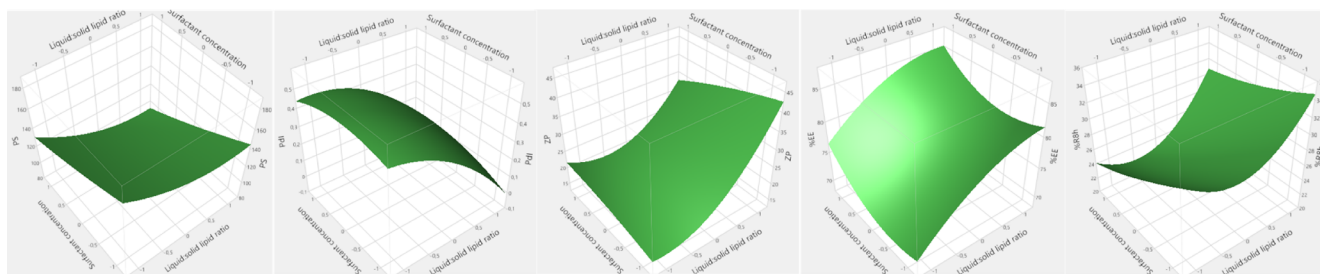
Fig. 5. Response surfaces for the two more significant factors at each fitted mathematical model.
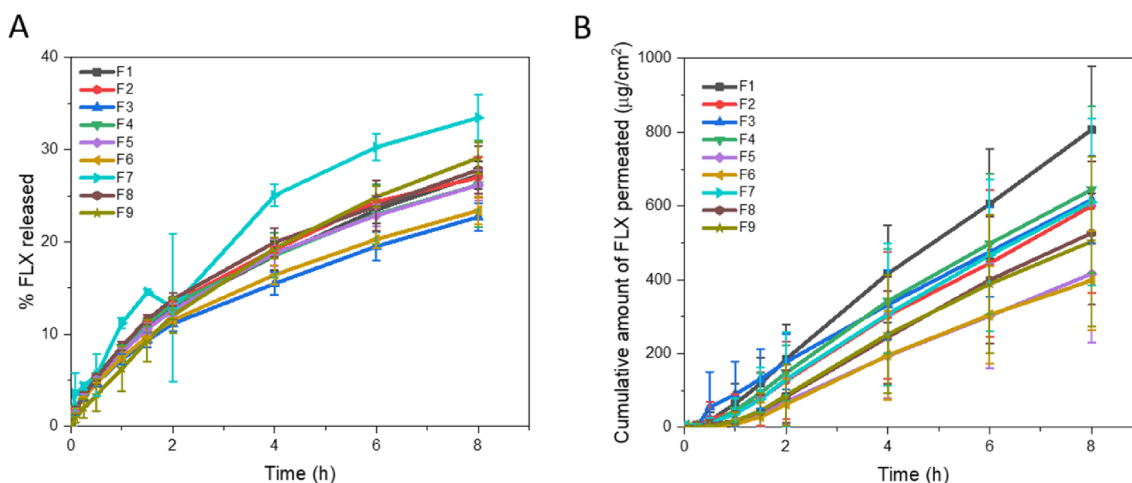
Fig. 6. (A) *In vitro* release and (B) *ex vivo* permeation profiles of FLX (mean $\pm$ SD, $n = 3$ and $n = 6$, respectively).

Even though Transcutol® HP ensures a statistically significant ($p < 0.0001$) higher solubility, its reduced viscosity, low partition coefficient (log P = -0.5) and consequent water miscibility may compromise FLX entrapment within the lipid matrix, ascribed to an early leakage into the aqueous phase. Hence, Lauroglycol™ 90 was selected as the liquid lipid for the preparation of lipid nanoparticles.

3.2. Optimization of the lipid nanoparticle preparation

The optimal conditions for the preparation of lipid nanoparticles were selected using a three-level, two-variable, 3^k full factorial planning. For that, the most CMAs were identified, based on the risk assessment analysis and included the liquid:solid lipid ratio and the emulsifier concentration (Table 1). Since Tween® 80 was a fixed parameter, despite the criticality attributed, it was not considered a CMA. This choice relied on two composition variables, one with influence on the inner phase behaviour, the liquid:solid lipid ratio, and another related to the external phase, with impact on the interface stabilization, the emulsifier concentration.

Note that the ratio of liquid lipid (oil) to solid lipid previously screened was optimized aiming at (i) maximizing the oil concentration (since oil is typically found to have higher drug solubility), (ii) producing a lipid mix with sufficient melting point to ensure the matrix solid state (consequently resulting in a sustained drug release), and (iii) enhancing the intranasal FLX permeation. Such approach allowed obtaining different types of nanocarrier systems, ranging from nanostructured lipid carriers (NLC) to nanoemulsions. Tween® 80 was selected as the surfactant for the preparation of lipid nanoparticles because of its good emulsification efficacy and biocompatible nature for the solid lipid liquid mix [18,42]. Surfactant concentration was optimized envisioning the nanosystem stabilization, without compromising its colloidal and loading properties (i.e. balance between smaller size and maximum percentage of entrapped FLX).

An array of quality parameters was defined as CQAs and comprehensively investigated, ranging from formulation physicochemical characterization (including colloidal and loading properties) to intranasal performance assessment (rheological, release, permeation) as depicted in Table 4. The integrated analysis of these responses yielded distinct models whose coefficient values are presented in Table 5. To perform an in-depth interpretation of each model, it is important to consider that a higher coefficient magnitude indicates a stronger effect of the CMA on the CQA, whilst a negative coefficient bears the opposite trend. In other words, the influence of a factor increases as the coefficient enhances, either positively or negatively [18,21].

An overall analysis of the models indicates that a better fitting was retrieved from the colloidal properties (particle size, polydispersity index, and zeta potential), followed by loading properties (entrapment efficiency) and lastly the performance parameters (release and permeation outcomes). This is in agreement with Fig. 4, which displays the observed vs. predicted values for CQA exhibiting a better goodness of fit. Moreover, Table 5 shows that isolated coefficient terms are, in the vast majority, statistically significant. Evaluation of ANOVA was also performed for model fitness (see supplementary material Table S3), revealing the suitability of the selected mathematical model for predicting the responses.

Scrutinizing the impact over lipid nanoparticle colloidal properties, it is observed that, regarding the decrease of the particle size, the increase in surfactant concentration from 2.5%w/V to 5%w/V (β2) assumes major relevance, followed by the increasing of liquid:solid lipid ratio (β1). On the other hand, the increase in zeta potential is mainly governed by the lipids ratio. In the case of loading properties, again, increasing the oil content in the lipid matrix resulted in higher FLX entrapment efficiency and loading capacity. Importantly, in what concerns the interaction term (β12), with the exception of polydispersity index and zeta potential, no significant interaction between both factors is apparent.
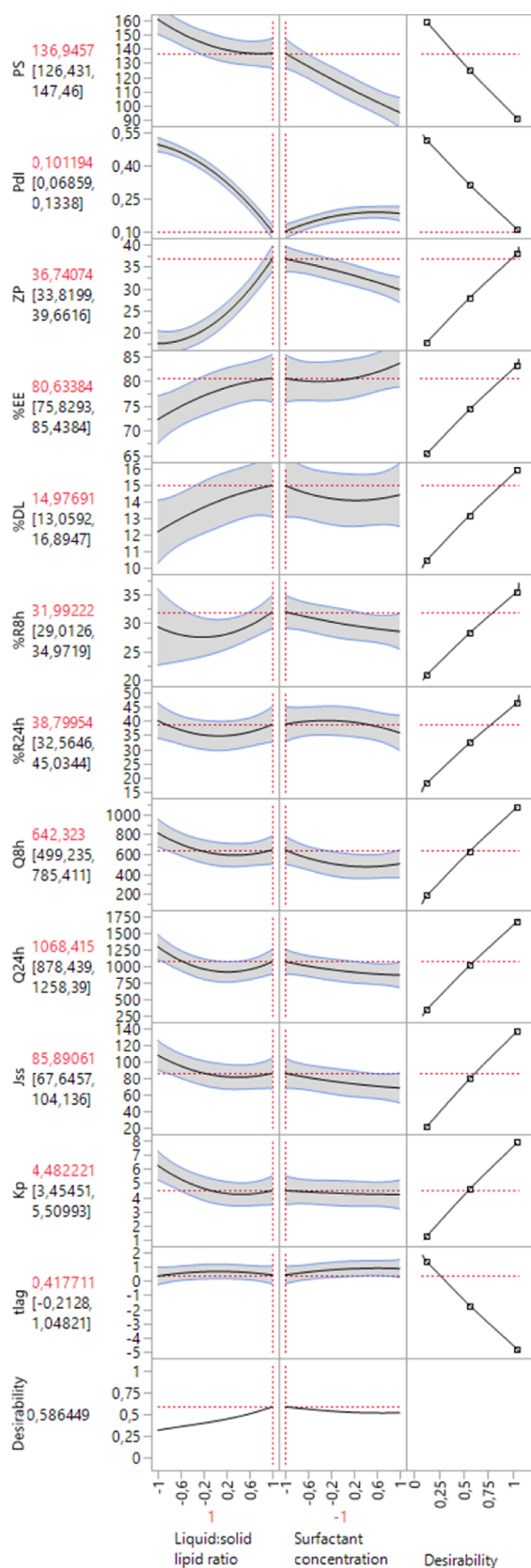
Fig. 7. Overall desirability for lipid nanoparticle composition optimization, according to the target (increase or decrease) imposed per CQA. The last row of plots shows the desirability trace for each factor. The overall desirability for all responses is defined as the geometric mean of the desirability functions for the individual responses.

Regarding intranasal performance, formulations containing a higher surfactant concentration tended to reduce FLX release extension and permeation rate. In the case of liquid:solid lipid ratio, a lower impact is generally observed. Interestingly, an increase in the oil content resulted in higher FLX release, in contrast to the reduction found in the permeation behaviour. No significant interaction between variables was evidenced. Such effects are consistent with the surface profiles, see Fig. 5.

When particularly concerning the release behaviour (Fig. 6A), formulations generally provided a sustained release of FLX, with approximately 30–40% of drug quantified at 24 h. F7, corresponding to the nanoemulsion, exhibited a lower retention of the drug within the lipid matrix, in contrast to the NLC formulations, which evidenced a more sustained FLX release. This trend could be ascribed to the liquid nature of the oily phase in the former, contrary to the solid lipid matrix found in the latter, which limits drug diffusion and increase the control over FLX delivery. Surprisingly, focusing on drug permeability through the porcine nasal olfactory epithelium (Fig. 6B), an inverse relationship was evident with the liquid:solid lipid amount. In other words, the formulation containing the highest amount of solid lipid concentration (F1) provided the highest permeability flux of FLX, followed by F4 and F7, all of them containing the lowest surfactant concentration (2.5%, w/V). Such behaviour could be ascribed to the higher crystallinity of NLC matrix, along with the increased viscosity, consequently rendering a closer contact with the epithelium. This will enable a better *in vivo* deposition pattern throughout the nasal mucosa with the retention of the formulation for a prolonged period of time, in contrast to the deformability found in the NE. This trend is in agreement with the rheological assessment (see Table 4), and the respective thermal behaviour (see Section 3.4). Moreover, a reduction in latency time was also observed, which is critical to ensure a faster therapeutic onset.

Summing-up, the increase in amount of liquid lipid and surfactant concentration yielded lower particles sizes and narrower size distributions. In turn, a higher stability was denoted as observed by the larger value of zeta potential values, along with enhanced loading properties.

Aiming at targeting (maximize or minimize, accordingly) all CQAs, the desirability approach was employed for CMA optimization. After conducting experiments and fit response models for all k responses, the desirability approach involves the following steps: (i) defining individual desirability functions for each response (di(Yi)), (ii) maximizing the overall desirability with respect to the controllable factors [43]. The desirability (D) function is described as the weighted geometric mean for several responses, or alternatively, a value comprised between 0 and 1 per response. A value of D different from zero indicates that all responses are in a desirable range, whilst a value close to 1 is pointed out as the combination of the different criteria considered optimal. As such, when D = 1, it means that the response values are close to the target ones [44–46]. Inspecting Fig. 7, it can be seen that the maximum desirability (0.586) was found for the formulation containing the highest liquid:solid lipid ratio (level 1, 100:0) and the lowest surfactant concentration (level −1, 2.5%w/V).

3.3. Stability testing

The rational design of a formulation is not complete without stability testing. Formulation stability is one of the key properties of quality that should be monitored. Indeed, ensuring that the state of a dispersion is maintained throughout the lifecycle of the product is demanding. It implies controlling any type of phase separation, including sedimentation or creaming, since these phenomena can impair the safety and efficacy of a formulation [47].

Apart from particle charge (zeta potential), size and nanoparticle growth control, the stability of a dispersion can be inferred by analytical centrifugation, through the analysis of transmission profiles, instability indices and velocity of particle separation. These are parameters obtained under accelerated gravitational field that ultimately
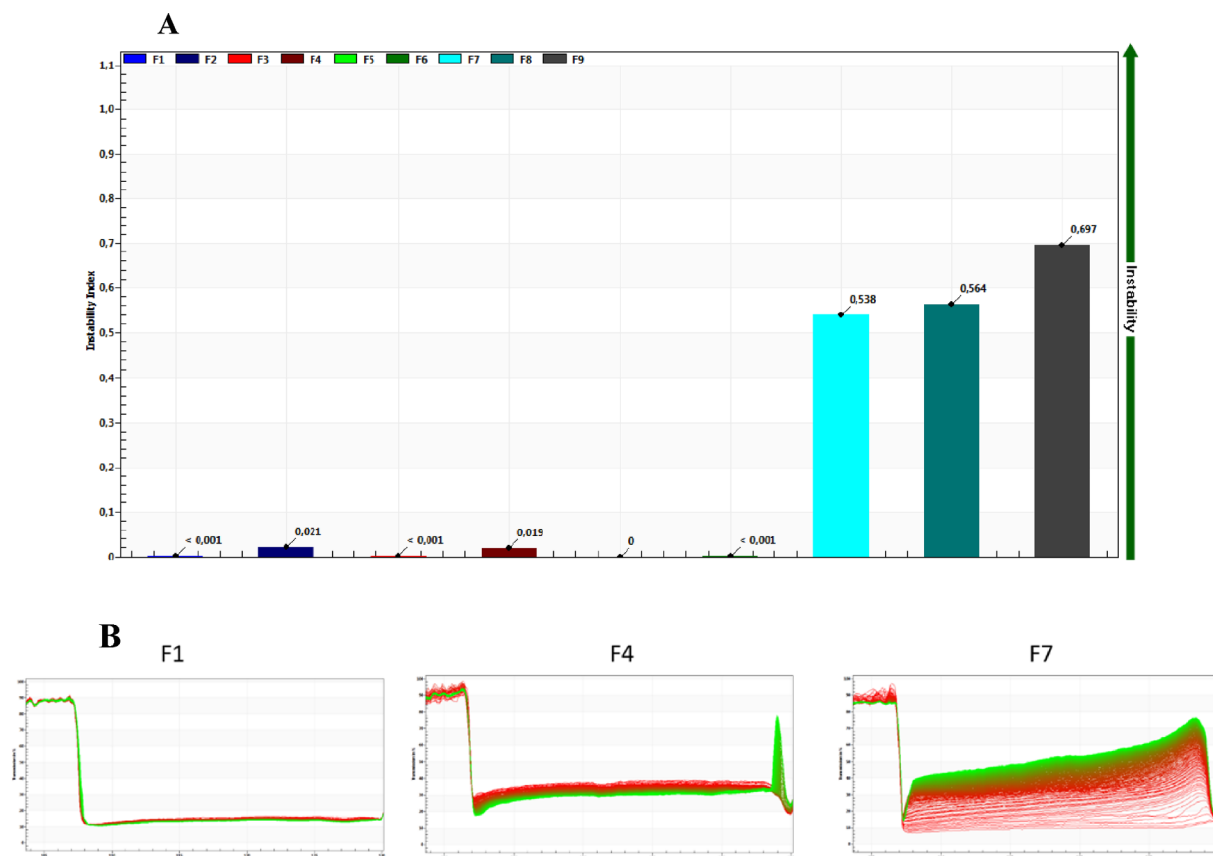
Fig. 8. Effect of the CMAs on the physical stability of the formulations, using analytical centrifugation to predict potential destabilization processes. A) Instability indices of F1-F9; B) Transmission profiles of F1, F4 and F7 formulations elucidating the impact of liquid:solid lipid ratio. Note that only profiles considering the lower surfactant concentration (level −1, 2.5% w/V) are herein presented, since this corresponds to the previously established optimal conditions.

Table 6
Velocity of separation of F1-F9 formulations.

Formulations	Velocity of separation (μm/s)
F1	1.721
F2	5.208
F3	1.270
F4	1.569
F5	2.287
F6	1.945
F7	−1.319
F8	−1.932
F9	−9.578

aids in a quick comparison of formulation shelf-life rather than waiting long-time at earth gravitation.

Considering the results obtained from the instability index (Fig. 8A), it can be observed that nanoemulsion formulations (F7-F9) are the most unstable. Conversely, formulations containing solid lipid, either in a 50:50 or 75:25 liquid:solid lipid ratio, exhibit an acceptable stability, as revealed by the lower instability index values (< 0.021). Undoubtedly, the lipid composition is the major factor influencing stability, as displayed in the transmission profiles (Fig. 8B). This trend is, however, opposite to zeta potential results, which evidenced a higher stability for NE formulations. Such behavior reflects the impact of liquid nature of the formulations, being consistent with the previous permeation findings.

Table 6 displays the velocity of particle separation. Distinct destabilization can be noted, with NLC (F1-F6) formulations exhibiting

sedimentation patterns, whilst NE (F7-F9) ones depict creaming formation (as extracted by the negative values of velocity of separation and clarification zone provided in the transmission profiles). Despite the instability ascertained for nanoemulsions, the transmission patterns displayed in Fig. 8B are characteristic of samples with unimodal distributions, which points out to the formulation homogeneity already described according to the PdI values (see Table 4).

Therefore, gathering the information retrieved from lipid nanoparticle characterization and based on the best performance in terms of nasal permeability enhancement, F1, F4 and F7 formulations were selected to further inspect their crystallinity, structure and morphology, as well as their biosafety.

3.4. Additional structural aspects

In what pertains thermal behaviour, DSC curves of FLX and respective formulations are displayed in Fig. 9A. Precirol® exhibits a melting peak at ca. 50 °C presenting a small shoulder, which may indicate the existence of other polymorphic forms. With the exception of plain and FLX-loaded F7 (nanoemulsions), all DSC formulation curves evidence this characteristic peak, although remained smaller and broader after particle preparation. This is compatible with the fact that the high aspect-ratio of particles leads to increased surface energy, thus creating an energetically suboptimal state, consequently reflected in a reduction in the melting point [48]. The DSC thermogram of FLX showed only one distinct endothermic peak at 160.7 °C, corresponding to its melting temperature [49]. This thermal transition is absent in the thermograms of the loaded formulations, corroborating its molecular
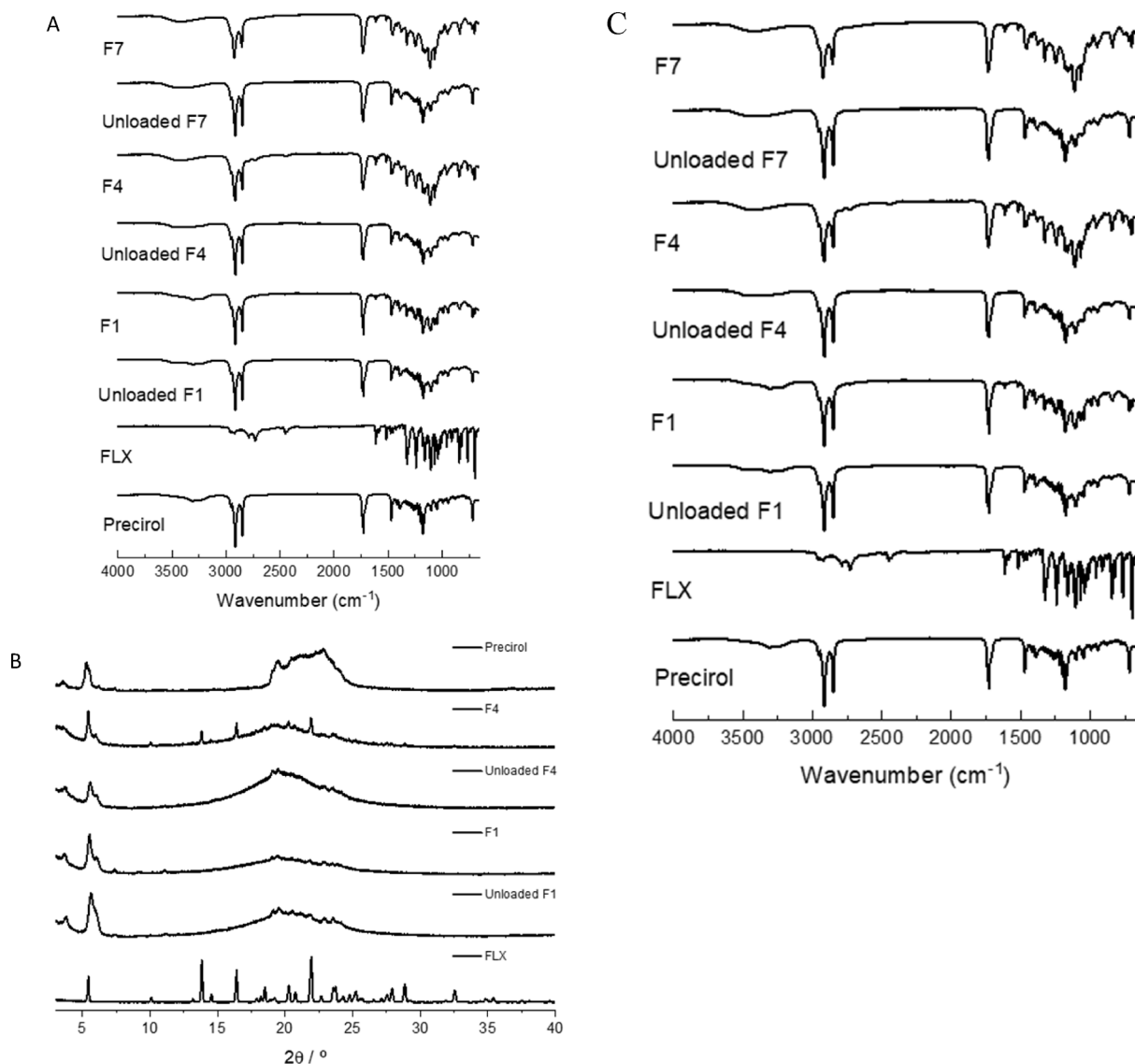
Fig. 9. A) DSC thermograms, B) X-ray diffractograms, and C) ATR-FTIR spectra of pure compounds (Precirol®, and fluoxetine hydrochloride), unloaded formulations and FLX-loaded formulations (F1, F4, and F7). Note that, since only solid samples are allowed for XRD analysis, the formulation F7, corresponding to the nanoemulsion was not considered for analysis.

Table 7
DSC melting characteristics of LN formulations and pure compounds.

Pure Compounds/LN formulations	T_{onset} (°C)	T_{peak} (°C)	Enthalpy of fusion (J/g)
Precirol®	49.8	61.9	165.21
Fluoxetine hydrochloride	156.9	160.7	107.07
Unloaded F1	43.8	52.1	68.00
F1	47.1	54.8	57.04
Unloaded F4	39.7	48.2	29.86
F4	38.6	48.7	24.91
Unloaded F7	–	–	–
F7	–	–	–

dispersion in the lipid matrix. Moreover, the decline in enthalpy detected in case of Precirol-based LNs, Table 7, points out to the formation of less ordered crystals or amorphous structures as crystalline substances are expected to require more energy to overcome lattice forces

[50].

Such observations are consistent with the XRD spectra analysis (Fig. 9B). Accordingly, the diffraction peaks typical from FLX (2θ of 5.43°, 10.89°, 13.83°, 16.40°, 21.52°, and 21.93°), with the exception of F4, are not evident in the loaded formulations. In turn, diffractograms essentially garner crystalline aspects ascribed to the solid lipid, Precirol®.

The intermolecular interactions in the different formulations were also monitored by ATR-FTIR, so as to complement information obtained from DSC and X-Ray diffraction (Fig. 9C). The Precirol® spectrum is characterized mainly by 3 important peaks, identified at 1737 cm^{-1} (C-O stretch), 1729.72 cm^{-1} and 1471.63 cm^{-1} (C-C stretching), and 2872 and 2849 cm^{-1} (C-H stretching), as previously reported [51]. This absorption peaks essentially reflect the molecular signature of the formulation spectra. IR spectrum of pure FLX shows 2957.35 cm^{-1} and 2919.27 cm^{-1} (asymmetric CH_2 and CH_3 stretches), 2789.92 cm^{-1}, 2729.81 cm^{-1} and 2450.62 cm^{-1} ($NH_2{}^{+}$–NH stretches), 1616.7 cm^{-1}, 1585.6 cm^{-1}, 1516.9 cm^{-1} and 1325 cm^{-1} (phenyl ring vibrations),
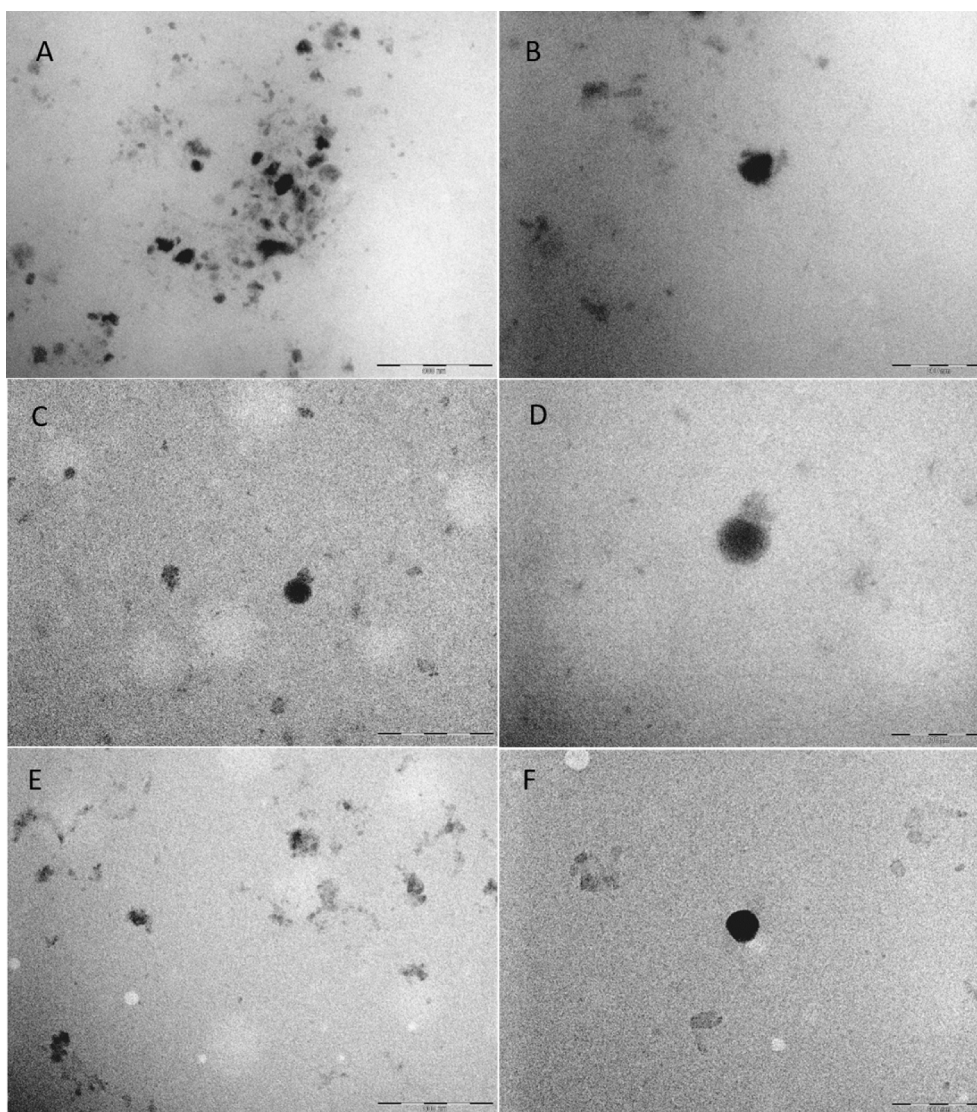
Fig. 10. TEM micrographs of F1 (A and B), F4 (C and D), and F7 (E and F) formulations.
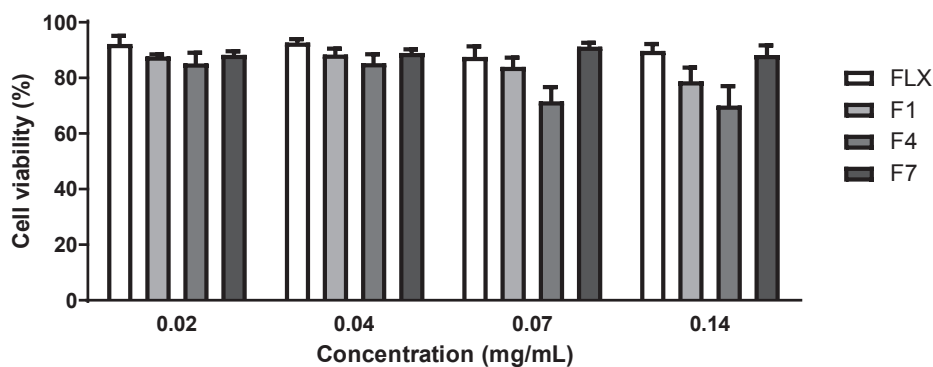
Fig. 11. *In vitro* effect of free FLX and FLX loaded lipid nanoparticles (F1, F4 and F7) on the viability of nasal squamous epithelium (RPMI 2650) cells. Concentration is expressed in relation to FLX. Data are expressed as mean ± SD ($n = 3$, in triplicate). ** $p < 0.01$, *** $p < 0.001$ in relation to the control, as extracted from two-way analysis of variance (ANOVA), with a Bonferroni multiple comparison test.

and 1240.8 cm^{-1} (C-O stretch) [52]. Similar to DSC and XRD findings, absorption peaks ascribed to FLX are not observed in FTIR spectra.

Fig. 10 illustrates TEM micrographs of FLX-loaded F1, F4 and F7, corresponding to NLC (50:50), NLC (75:25) and nanoemulsion (100:0) formulations, respectively. Essentially, particles appear spherical with smooth surface and relatively uniform size distribution. Particle diameter recorded by TEM are consistent with size measurements by DLS. Noteworthy, the absence of drug crystals in the TEM micrographs

suggests favourable entrapment of FLX within lipid matrix during particle formation, in accordance with the EE and DL values obtained (Table 4).

3.5. Cytotoxicity assessment

F1, F4 and F7 formulations were additionally selected to further inspect their biosafety *in vitro*.

Table 8
IC$_{50}$ of LN formulations incubated with RPMI 2650 cell line for 24 h. Values are estimated in relation to the total lipid content.

Formulations	IC$_{50}$ (mg/mL)*
Unloaded F1	0.80 ± 0.03
F1	0.320 ± 0.004
Unloaded F4	0.45 ± 0.01
F4	0.165 ± 0.005
Unloaded F7	0.46 ± 0.02
F7	0.48 ± 0.01

First, the influence of FLX on the viability of RPMI 2650 cells was assessed either in solution or encapsulated in the lipid nanoparticle. These tests were performed within the drug therapeutic range and the results revealed that cell viability remained practically unchanged in relation to the control, with the exception of F4 at the two highest concentrations (Fig. 11). Nevertheless, the relative cell viability in the presence of F4 remained above 70% and, as such, it is considered non-cytotoxic [53].

The toxicity of empty lipid nanoparticles and FLX-loaded lipid nanoparticles, given by IC$_{50}$ values (Table 8), demonstrates that, in general, drug incorporation into lipid nanoparticles decreases cell viability, when compared to the plain nanoparticles. Unloaded and loaded F4 formulations exhibited the lowest IC$_{50}$ values, corroborating their higher impact on cell viability. Taking into consideration the favorable cell viability and stability profile, F1, the formulation containing the higher amount of solid lipid, was selected to proceed to the behavioral evaluation.

3.6. Behavioral in vivo evaluation

In an attempt to elucidate the treatment response underlying psychiatric illness, two complementary behavioral tests were performed to assess antidepressant and anxiolytic effects: the FST and the MBT, respectively.

The FST is a rodent behavioral test employed for evaluating depressive-like states, useful for the assessment of the efficacy of antidepressant drugs. Accordingly, mice are placed in an inescapable transparent tank filled with water and their escape related mobility behavior, as well as the swimming motion reflect a measure of behavioral despair [37]. In turn, the rodent MBT is often applied as a measure of anxiety- and compulsive-like behaviors, wherein more covered marbles denote an exacerbation of the anxiety effect.

Fig. 12A revealed higher mobility time for the groups that received

FLX by intranasal delivery of F1 formulation or FLX solution by oral gavage, relatively to untreated animals (control group). Even though no statistical difference was observed, these findings suggest that antidepressant activity occurs independently of the administration route. Nonetheless, it seems to be higher when FLX solution is orally administered, since the immobility time is lower than that of intranasal group. Moreover, the intranasal group did not improve climbing time as it was expected. Such trends could somewhat reflect (i) the sustained drug release profile, (ii) schedule of test execution, and (iii) the liquid nature of F1. Addressing the former, and according to the previously reported data, brain concentrations are expected to be reduced. Moreover, brain maximal concentrations after intranasal administration are typically achieved within the first 15 min. Since the test was carried out one-hour post-treatment, a prominent benefit of the intranasal administration in relation to oral delivery may be no longer visible. In turn, the liquid nature of F1 may condition its full retention in the superior respiratory tract, with consequent avoidance of pulmonary deposition. Its performance might be improved if further included in a proper jellified vehicle, e.g. thermoreversible nasal gel [54].

The effect of FLX administered intranasally or by oral gavage is corroborated by the inhibition percentage registered in both behavioral tests (Fig. 12B). Interestingly, besides the increase observed regarding FST immobility inhibition relatively to non-treated animals, both animal groups that received intranasal or oral treatments covered less marbles than non-treated animals. Furthermore, the group administered with F1 intranasal formulation exhibited higher inhibition percentage on MBT than the orally administered animal group (37 ± 14% versus 21 ± 15%), eliciting a larger mitigation of anxiety-like behavior, similarly to that reported by Kobayashi et al. [31].

4. Conclusions

In this work, a lipid nanoparticle formulation for encapsulating antidepressant drugs was successfully designed. "Get it right at the first time" was the approach considered by employing the QbD perspective, taking into consideration the correlations observed among liquid:solid lipid ratio and surfactant concentration, as critical material variables, on 12 distinct critical quality attributes for intranasal drug delivery. Above all, it was observed that only a combinatorial approach encompassing physicochemical and performance variables can provide enough information to robustly support a better decision in what concerns formulation optimization.

In vitro permeation and in vivo behavioral results showed that, in line with the original hypothesis, lipid nanoparticles could fit the purpose of provisioning similar antidepressant and anxiolytic effects to
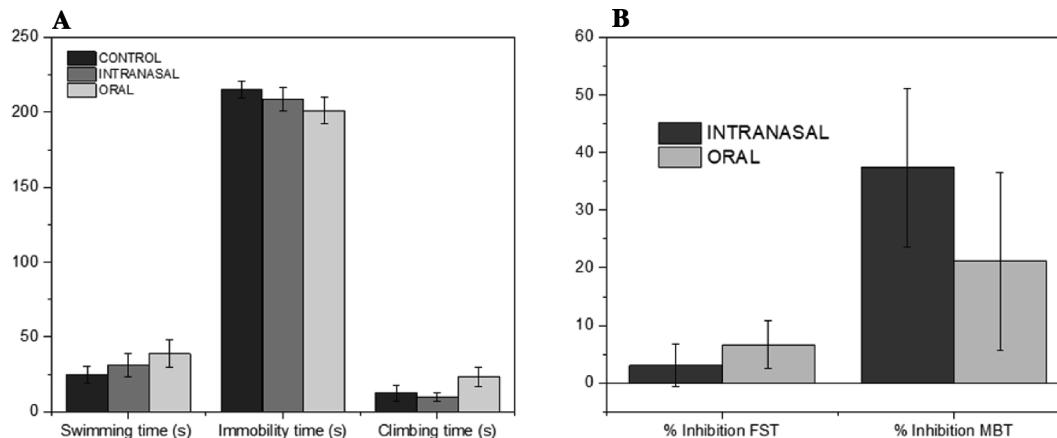
Fig. 12. (A) Immobility time, mobility time and climbing time (in seconds) in the Forced Swim Test (FST), one hour after a single administration of F1 by intranasal route, FLX oral solution and non-treated (control) animals ($n = 7$). (B) Inhibition percentage obtained from the FST and Marble-burying test (MBT). Results are expressed as mean ± SEM.

those achieved after administration of the oral solution. As such, it consubstantiates that the dual lipid nanoparticles-intranasal delivery strategy herein investigated may be tailored to provide a sustained drug release ultimately compatible with a prolonged and more effective antidepressant effect.

Acknowledgements

Appendix A. Supplementary material

Supplementary data to this article can be found online at https://doi.org/10.1016/j.ejpb.2020.04.011.

References

[1] WHO, Depression, in, 2018.
[2] O.F. O'Leary, T.G. Dinan, J.F. Cryan, Faster, better, stronger: towards new antidepressant therapeutic strategies, Eur. J. Pharmacol. 753 (2015) 32–50.
[3] Mordorintelligence, Global Antidepressant Market, in, 2018.
[4] M.Y. Sum, J. Sim, K. Sim, R.J. Baldessarini, W.K. Lau, Prevention of relapse and recurrence in adults with major depressive disorder: systematic review and meta-analyses of controlled trials, Int. J. Neuropsychopharmacol. 19 (2015).
[5] A. Forte, R.J. Baldessarini, L. Tondo, G.H. Vazquez, M. Pompili, P. Girardi, Long-term morbidity in bipolar-I, bipolar-II, and unipolar major depressive disorders, J. Affect Disord. 178 (2015) 71–78.
[6] H. Akil, J. Gordon, R. Hen, J. Javitch, H. Mayberg, B. McEwen, M.J. Meaney, E.J. Nestler, Treatment resistant depression: a multi-scale, systems biology approach, Neurosci. Biobehav. Rev. 84 (2018) 272–288.
[7] D. Bennabi, T. Charpeaud, A. Yrondi, J.B. Genty, S. Destouches, S. Lancrenon, N. Alaili, F. Bellivier, T. Bougerol, V. Camus, J.M. Dorey, O. Doumy, F. Haesebaert, J. Holtzmann, C. Lancon, M. Lefebvre, F. Moliere, I. Nieto, C. Rabu, R. Richieri, L. Schmitt, F. Stephan, G. Vaiva, M. Walter, M. Leboyer, W. El-Hage, P.M. Llorca, P. Courtet, B. Aouizerate, E. Haffen, Clinical guidelines for the management of treatment-resistant depression: French recommendations from experts, the French Association for Biological Psychiatry and Neuropsychopharmacology and the fondation FondaMental, BMC psychiatry 19 (2019) 262.
[8] J.P. Pandarakalam, Challenges of treatment-resistant depression, Psychiatria Danubina 30 (2018) 273–284.
[9] B.N. Gaynes, L. Lux, G. Gartlehner, G. Asher, V. Forman-Hoffman, J. Green, E. Boland, R.P. Weber, C. Randolph, C. Bann, E. Coker-Schwimmer, M. Viswanathan, K.N. Lohr, Defining treatment-resistant depression, Depress. Anxiety, 12.
[10] A. Mistry, S. Stolnik, L. Illum, Nanoparticles for direct nose-to-brain delivery of drugs, Int. J. Pharm. 379 (2009) 146–157.
[11] A.R. Khan, M. Liu, M.W. Khan, G. Zhai, Progress in brain targeting drug delivery system by nasal route, J. Controlled Release: Off. J. Controlled Release Soc. 268 (2017) 364–389.
[12] M. Van Woensel, N. Wauthoz, R. Rosière, K. Amighi, V. Mathieu, F. Lefranc, S.W. Van Gool, S. De Vleeschouwer, Formulations for intranasal delivery of pharmacological agents to combat brain disease: a new opportunity to tackle GBM? Cancers 5 (2013) 1020.
[13] L. Illum, Transport of drugs from the nasal cavity to the central nervous system, Eur. J. Pharm. Sci. 11 (2000) 1–18.
[14] C. Vitorino, J. Almeida, L.M. Gonçalves, A.J. Almeida, J.J. Sousa, A.A.C.C. Pais, Co-encapsulating nanostructured lipid carriers for transdermal application: from experimental design to the molecular detail, J. Control. Release 167 (2013) 301–314.
[15] M. Mendes, H.T. Soares, L.G. Arnaut, J.J. Sousa, A.A.C.C. Pais, C. Vitorino, Can lipid nanoparticles improve intestinal absorption? Int J Pharm 515 (2016) 69–83.
[16] F.E. O'Brien, T.G. Dinan, B.T. Griffin, J.F. Cryan, Interactions between antidepressants and P-glycoprotein at the blood-brain barrier: clinical significance of in vitro and in vivo findings, Br. J. Pharmacol. 165 (2012) 289–312.
[17] S. Thümmler, E. Dor, R. David, G. Leali, M. Battista, A. David, F. Askenazy, C. Verstuyft, Pharmacoresistant severe mental health disorders in children and adolescents: functional abnormalities of cytochrome P450 2D6, Front. Psychiatry 9 (2018).
[18] C. Vitorino, J. Almeida, L.M. Goncalves, A.J. Almeida, J.J. Sousa, A.A. Pais, Co-encapsulating nanostructured lipid carriers for transdermal application: from experimental design to the molecular detail, J. Controlled Release: Off. J. Controlled Release Soc. 167 (2013) 301–314.
[19] A. Barone, M. Mendes, C. Cabral, R. Mare, D. Paolino, C. Vitorino, Hybrid nanostructured films for topical administration of simvastatin as coadjuvant treatment of melanoma, J. Pharm. Sci. (2019).
[20] M. Mendes, A. Miranda, T. Cova, L. Goncalves, A.J. Almeida, J.J. Sousa, M.L.C. do Vale, E.F. Marques, A. Pais, C. Vitorino, Modeling of ultra-small lipid nanoparticle surface charge for targeting glioblastoma, Eur. J. Pharma. Sci.: Off. J. Eur. Feder. Pharm. Sci. 117 (2018) 255–269.
[21] J. Basso, M. Mendes, T.F.G.G. Cova, J.J. Sousa, A.A.C.C. Pais, C. Vitorino, Analytical Quality by Design (AQbD) as a multiaddressable platform for co-encapsulating drug assays, Anal. Methods 10 (2018) 5659–5671.
[22] R. Ana, M. Mendes, J. Sousa, A. Pais, A. Falcao, A. Fortuna, C. Vitorino, Rethinking carbamazepine oral delivery using polymer-lipid hybrid nanoparticles, Int. J. Pharm. 554 (2019) 352–365.
[23] M. Yerramilli, S. Ghosh, Long-term stability of sodium caseinate-stabilized nanoemulsions, J. Food Sci. Technol. 54 (2017) 82–92.
[24] Y.-T. Hu, Y. Ting, J.-Y. Hu, S.-C. Hsieh, Techniques and methods to study functional characteristics of emulsion systems, J. Food Drug Anal. 25 (2017) 16–26.
[25] ISO, Guidelines for the characterization of dispersion stability, ISO/TR13097:2013, in, 2013.
[26] D. Lerche, T. Sobisch, Direct and accelerated characterization of formulation stability, J. Dispersion Sci. Technol. 32 (2011) 1799–1811.
[27] J. O'Brien, I. Wilson, T. Orton, F. Pognan, Investigation of the Alamar Blue (resazurin) fluorescent dye for the assessment of mammalian cell cytotoxicity, Eur. J. Biochem. 267 (2000) 5421–5426.
[28] ISO-10993-5:2009(E), Biological evaluation of medical devices, in: International Organization for Standardization.
[29] K.u. Njung'e, S.L. Handley, Evaluation of marble-burying behavior as a model of anxiety, Pharmacol. Biochem. Behavior 38 (1991) 63–67.
[30] W. Wolmarans de, D.J. Stein, B.H. Harvey, Of mice and marbles: Novel perspectives on burying behavior as a screening test for psychiatric illness, Cogn. Affect Behav. Neurosci., 16 (2016) 551–560.
[31] G. de Brouwer, W. Wolmarans, Back to basics: a methodological perspective on marble-burying behavior as a screening test for psychiatric illness, Behav. Processes 157 (2018) 590–600.
[32] M. Kalariya, R. Prajapati, S.K. Parmar, N. Sheth, Effect of hydroalcoholic extract of leaves of Colocasia esculenta on marble-burying behavior in mice: implications for obsessive–compulsive disorder, Pharm. Biol. 53 (2015) 1239–1242.
[33] T. Kobayashi, E. Hayashi, M. Shimamura, M. Kinoshita, N.P. Murphy, Neurochemical responses to antidepressants in the prefrontal cortex of mice and their efficacy in preclinical models of anxiety-like and depression-like behavior: a comparative and correlational study, Psychopharmacology (Berl) 197 (2008) 567–580.
[34] R.D. Porsolt, A. Bertin, M. Jalfre, Behavioral despair in mice: a primary screening test for antidepressants, Archives internationales de pharmacodynamie et de therapie 229 (1977) 327–336.
[35] Y. Hao, H. Ge, M. Sun, Y. Gao, Selecting an appropriate animal model of depression, Int. J. Mol. Sci. 20 (2019).
[36] J.M. Deussing, Animal models of depression, Drug Discovery Today: Disease Models 3 (2006) 375–383.
[37] A. Can, D.T. Dao, M. Arad, C.E. Terrillion, S.C. Piantadosi, T.D. Gould, The mouse forced swim test, J. Visual. Exp.: JoVE (2012) e3638.
[38] R. Yankelevitch-Yahav, M. Franko, A. Huly, R. Doron, The forced swim test as a model of depressive-like behavior, J. Visual. Exp.: JoVE (2015).
[39] A. Simoes, F. Veiga, A. Figueiras, C. Vitorino, A practical framework for implementing Quality by Design to the development of topical drug products: nanosystem-based dosage forms, Int. J. Pharm. 548 (2018) 385–399.
[40] M. Yasir, U.V.S. Sara, Solid lipid nanoparticles for nose to brain delivery of haloperidol: in vitro drug release and pharmacokinetics evaluation, Acta Pharmaceutica Sinica B 4 (2014) 454–463.
[41] H.M. Aboud, M.H. El komy, A.A. Ali, S.F. El Menshawe, A. Abd Elbary, Development, Optimization, and evaluation of carvedilol-loaded solid lipid nanoparticles for intranasal drug delivery, AAPS PharmSciTech, 17 (2016) 1353–1365.
[42] M. Yasir, U.V.S. Sara, I. Chauhan, P.K. Gaur, A.P. Singh, D. Puri, A. , Solid lipid nanoparticles for nose to brain delivery of donepezil: formulation, optimization by Box–Behnken design, in vitro and in vivo evaluation, Artificial cells, Nanomed., Biotechnol. 46 (2018) 1838–1851.
[43] Multiple responses: The desirability approach, in.
[44] M. Miranda, A. Pais, C. Cardoso, C. Vitorino, aQbD as a platform for IVRT method development-A regulatory oriented approach, Int. J. Pharm. 118695 (2019).
[45] P.D. Kalariya, D. Namdev, R. Srinivas, S. Gananadhamu, Application of experimental design and response surface technique for selecting the optimum RP-HPLC conditions for the determination of moxifloxacin HCl and ketorolac tromethamine in eye drops, J. Saudi Chem. Soc. 21 (2017) S373–S382.
[46] S. Kamboj, V. Rana, Quality-by-design based development of a self-microemulsifying drug delivery system to reduce the effect of food on Nelfinavir mesylate, Int. J. Pharm. 501 (2016) 311–325.
[47] K. Pathak, S. Pattnaik, Stability testing parameters and issues for nanotechnology-based drug products, in: S. Bajaj, S. Singh (Eds.), Methods for Stability Testing of Pharmaceuticals, Springer, New York, New York, NY, 2018, pp. 293–305.
[48] S. Makled, N. Nafee, N. Boraie, Nebulized solid lipid nanoparticles for the potential treatment of pulmonary hypertension via targeted delivery of phosphodiesterase-5-inhibitor, Int. J. Pharm. 517 (2017) 312–321.

[49] M.A.S. Silva, R.G. Kelmann, T. Foppa, A.P. Cruz, C.D. Bertol, T. Sartori, A. Granada, F. Carmignan, F.S. Murakami, Thermoanalyticalstudy of fluoxetine hydrochloride, J. Therm. Anal. Calorim. 87 (2007) 463–467.

[50] Z. Li, L. Yu, L. Zheng, F. Geng, Studies on crystallinity state of puerarin loaded solid lipid nanoparticles prepared by double emulsion method, J. Therm. Anal. Calorim. 99 (2010) 689–693.

[51] D.D. Kumbhar, V.B. Pokharkar, Engineering of a nanostructured lipid carrier for the poorly water-soluble drug, bicalutamide: physicochemical investigations, Colloids Surf., A 416 (2013) 32–42.

[52] D.S. Risley, R.J. Bopp, Fluoxetine, in: K. Florey (Ed.), Analytical Profiles of Drug Substances, Academic Press, 1990, pp. 193–219.

[53] ISO10993-5:2009, Biological evaluation of medical devices — Part 5: Tests for in vitro cytotoxicity, in.

[54] A. Serralheiro, G. Alves, A. Fortuna, A. Falcao, Intranasal administration of carba-mazepine to mice: a direct delivery pathway for brain targeting, Eur. J. Pharm. Sci.: Off. J. Eur. Feder. Pharm. Sci. 60 (2014) 32–39.